Uzbek Journal "Problems of Mechanics"

Research Article

DOI: 10.68846/pmjournal-2026-37-00005

Diffraction of an SH wave by a filled elliptic cylinder in a viscoelastic medium

R.A. Sabirova[1*]

[1] Tashkent Institute of Chemical Technology, Tashkent, 100011, Uzbekistan

[*] **Corresponding author:** r.sabirova@tkti.uz

Received: 21 June 2026 | **Revised:** 15 August 2026 | **Accepted:** 05 September 2026 | **Published:** 30 September 2026

ABSTRACT

Diffraction of a time-harmonic SH wave by a filled elliptic cylinder in an unbounded viscoelastic medium with the Rzhanitsyn–Koltunov kernel is studied; the unfilled cavity is analysed first. The freezing method reduces the problem to a Helmholtz equation with a complex wavenumber, solved exactly in Mathieu functions of complex parameter. The algorithm is verified against the static limit, the circular-cavity solution and the method of fundamental solutions (agreement to 10^{-12}). Normalising the decaying incident wave at the origin overstates the dynamic stress concentration factor (DSCF) by up to 27%; normalisation at the point of first contact is proposed. The viscous effect is split into softening, which shifts the DSCF spectrum to lower frequencies by 37–45%, and damping, which reduces the DSCF by up to 15%. Near $k_0 a \approx 1$ the DSCF decreases by 14–29%, while its peak drops by only 1–5%. The kernel parameters A and α dominate, while β has little effect (below 1.5%). For a viscoelastic filler, the ratio of filler and medium viscosities governs the stress state: the interface stress at a stiff filler varies from −15% to +17%, the tangential stress at a soft filler from −17% to +24%.

KEYWORDS

viscoelastic medium, elliptic cavity, SH wave, diffraction, filler, Mathieu functions, Rzhanitsyn–Koltunov kernel, dynamic stress concentration.

1. Introduction

When assessing the seismic resistance of underground pipelines, tunnels and other structures, it is necessary to know the concentration of dynamic stresses around cavities. The cross-section of many real structures differs from a circle; therefore, the ellipse is the simplest yet practically important generalization: by varying the ratio b/a, shapes ranging from a circle to a crack can be covered. Classical results on wave diffraction by cylindrical cavities in an elastic medium are presented in monographs [1, 2].

The scattering of SH waves by elliptic cavities has been actively studied in recent years. Early results for an elliptic cavity at the interface of two media were obtained in [3]. In [4], the solution in Mathieu functions was extended to impact loading via the Fourier transform, and a strong influence of the incidence angle, the wavenumber and the ratio of the ellipse axes on the dynamic stress concentration factor (DSCF) was shown. A non-confocal lined elliptic tunnel [5], an inhomogeneous medium with varying density and modulus [6], gradient piezomagnetic materials [7], and the interaction of an elliptic cavity with a crack in anisotropic rock [8] were investigated by conformal mapping and wave function expansion methods. Mathieu functions are also used in problems of an elliptic hole in piezoelectric materials [9] and of a nanosized elliptic hole with surface effects [10]. Acoustic wave scattering by elliptic bodies was studied in [11–13], where the viscosity of the fluid was taken into account in [12, 13]. However, in most of these works the surrounding medium is considered elastic, and its hereditary properties are not taken into account.

The hereditary (viscoelastic) properties of soils and structural materials are described by the Boltzmann–Volterra integral operator [14, 15]. For harmonic processes, the "freezing" method proposed by A.N. Filatov [16] reduces the integro-differential equations to differential equations with complex coefficients. This approach was applied to cylindrical cavities in [17], to the assessment of the dissipative properties of hollow cylinders with a filler with the Rzhanitsyn–Koltunov kernel in [18], and to the diffraction of P-, SV- and SH-waves by elliptic cylinders in [19–21]. However, the influence of the kernel parameters on the DSCF was not systematically studied in these works. The influence of viscosity was not separated into the modulus reduction (softening of the medium) and damping contributions. The problem of normalizing the incident wave in a damping medium was not considered either.

The aim of this paper is to construct an exact solution of the problem of SH-wave diffraction by an elliptic cavity in a viscoelastic medium in Mathieu functions of complex parameter and to verify it by an independent method. It is also intended to estimate quantitatively the influence of the Rzhanitsyn–Koltunov kernel parameters on the DSCF frequency spectrum and to generalize the solution to a filled elliptic cylinder.

Scientific novelty. The same problem was solved in [19] for a single wavenumber ($k_s = 1.7$) and a single set of kernel parameters. No comparison with the elastic case or verification of the solution was given there. In this paper, the results of [19] were used and the following was done:

1) the solution was verified against the static limit, the exact solution for a circular cavity and the method of fundamental solutions (agreement up to 10^{-12});

2) it was shown that normalizing the incident wave at the coordinate origin in a damping medium artificially increases the DSCF by up to 27 %, and normalization at the point where the wave first touches the cavity was proposed;

3) the complete frequency spectrum of the DSCF ($0 < k_0 a \leq 6$) was obtained for the elastic and viscoelastic cases, and the influence of viscosity was separated into the modulus reduction (spectrum shift) and damping contributions;

4) the influence of each of the parameters A, α, β of the Rzhanitsyn–Koltunov kernel on the DSCF was estimated quantitatively;

5) the viscoelastic filled elliptic cylinder, which was not considered in [19], was solved, and the influence of the ratio of the filler and medium viscosities on the contact stress was determined. In [20], the antiplane deformation problem for a filled elliptic cylindrical shell was only formulated and reduced to the Mathieu equation: the boundary value problem was not solved, the stresses were not calculated and no numerical results were given.

2. Problem statement

An infinitely long elliptic cylindrical cavity with semi-axes a and b (a > b) is located in a homogeneous, isotropic, viscoelastic medium (Figure 1). A plane harmonic SH wave making an angle θ_0 with the x axis is incident on it. The points of the medium have only the displacement w(x, y, t) along the cylinder axis, i.e. the problem is one of antiplane deformation.

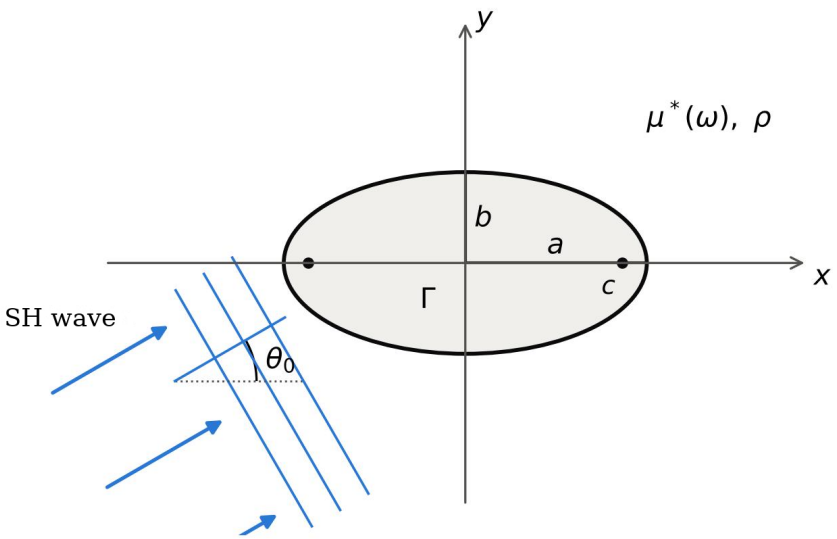


Figure 1. Computational scheme of the problem

The constitutive equation of the medium is written on the basis of the theory of hereditary elasticity:

$$\tau_{jz}(t) = \mu_0 \left[\gamma_{jz}(t) - \int_{-\infty}^{t} R(t-\tau)\, \gamma_{jz}(\tau)\, d\tau \right], \qquad j = x, y, \tag{1}$$

where μ_0 is the instantaneous shear modulus and R(t) is the relaxation kernel. The weakly singular three-parameter Rzhanitsyn–Koltunov kernel is taken as the kernel [14]:

$$R(t) = A\, e^{-\beta t}\, t^{\alpha-1}, \qquad A > 0, \quad \beta > 0, \quad 0 < \alpha < 1. \tag{2}$$

The kernel must satisfy the condition $\int_0^\infty R(t)\, dt = A\, \Gamma(\alpha)\, \beta^{-\alpha} < 1$. For a time-harmonic process $w = W(x, y)\, e^{-i\omega t}$, the "freezing" method [16] replaces the operator (1) by the complex modulus

$$\mu^*(\omega) = \mu_0 \left[1 - \Gamma_c(\omega) - i\, \Gamma_s(\omega) \right], \tag{3}$$

where Γ_c and Γ_s are the cosine and sine Fourier transforms of the kernel. For kernel (2) they have a closed form:

$$\Gamma_c(\omega) + i\, \Gamma_s(\omega) = \int_0^\infty R(t)\, e^{i\omega t}\, dt = \frac{A\, \Gamma(\alpha)}{\left(\beta^2 + \omega^2\right)^{\alpha/2}}\, e^{i\alpha\varphi}, \qquad \varphi = arctan\frac{\omega}{\beta}. \tag{4}$$

The equation of motion $\rho\, \partial^2 w/\partial t^2 = \partial \tau_{xz}/\partial x + \partial \tau_{yz}/\partial y$ reduces to the Helmholtz equation for the amplitude:

$$\nabla^2 W + k_*^2 W = 0, \qquad k_* = \frac{k_0}{\sqrt{1 - \Gamma_c - i\, \Gamma_s}}, \qquad k_0 = \frac{\omega}{c_0}, \qquad c_0 = \sqrt{\mu_0/\rho}. \tag{5}$$

Since $Im k_* > 0$, the wave decays in the direction of propagation. In the calculations, the dimensionless time $\bar{t} = t\, c_0/a$ is used; therefore, the dimensionless frequency equals $\bar{\omega} = k_0 a$, and the parameters of kernel (2) are given in the same units.

The elliptic coordinates (ξ, η) are introduced as follows:

$$x = c \cosh\xi \cos\eta, \qquad y = c \sinh\xi \sin\eta, \qquad c = \sqrt{a^2 - b^2}. \tag{6}$$

The cavity contour Γ corresponds to $\xi = \xi_0 = \tanh^{-1}(b/a)$. The contour is free of stresses:

$$\tau_{\xi z}|_{\xi=\xi_0} = \frac{\mu^*}{c\, J}\, \frac{\partial}{\partial \xi} \left(W^{(i)} + W^{(s)} \right)|_{\xi=\xi_0} = 0, \qquad J = \sqrt{\sinh^2\xi + \sin^2\eta}. \tag{7}$$

Here the incident wave is

$$W^{(i)} = W_0 \exp\left[i\, k_* \left(x \cos\theta_0 + y \sin\theta_0\right)\right], \tag{8}$$

and $W^{(s)}$ is the scattered wave, which satisfies the Sommerfeld radiation condition at infinity.

3. Solution method

In coordinates (6), Equation (5) is reduced by separation of variables to the angular and radial Mathieu equations:

$$\frac{d^2\Phi}{d\eta^2} + (\lambda - 2q\cos 2\eta)\,\Phi = 0, \qquad \frac{d^2\Psi}{d\xi^2} - (\lambda - 2q\cosh 2\xi)\,\Psi = 0, \qquad q = \left(\frac{k_* c}{2}\right)^2. \tag{9}$$

In a viscoelastic medium, the parameter q is complex. The angular functions $ce_m(\eta, q)$, $se_m(\eta, q)$ are sought in the form of Fourier series. For example, for the even-order functions:

$$ce_{2n}(\eta, q) = \sum_{r=0}^{\infty} A_{2r}^{(2n)} \cos 2r\eta, \tag{10}$$

where the coefficients are determined from the three-term recurrence relations:

$$\begin{aligned} \lambda A_0 &= q A_2, \qquad (\lambda - 4) A_2 = q\,(2A_0 + A_4), \\ \left(\lambda - 4r^2\right) A_{2r} &= q\,(A_{2r-2} + A_{2r+2}), \qquad r \geq 2. \end{aligned} \tag{11}$$

System (11) is solved as an eigenvalue problem for an N×N tridiagonal matrix. Here λ are the eigenvalues and A_{2r} are the components of the eigenvectors. Similar systems are constructed for the odd-order functions ce_{2n+1}, se_{2n+1} and the even se_{2n+2} [22–25]. In this approach, no ordering or classification of the eigenvalues is required for complex q, since only the completeness of the set of angular functions matters in the subsequent calculation.

The radial Mathieu–Hankel functions representing the scattered wave are calculated through series of products of Bessel functions [23]:

$$Mc_{2n}^{(3)}(\xi, q) = \frac{1}{\varepsilon_s A_{2s}} \sum_{r=0}^{\infty} (-1)^{r+n} A_{2r} \left[J_{r-s}(u_1)\; H_{r+s}^{(1)}(u_2) + J_{r+s}(u_1)\; H_{r-s}^{(1)}(u_2)\right], \tag{12}$$

where $u_1 = \sqrt{q}\, e^{-\xi}$, $u_2 = \sqrt{q}\, e^{\xi}$, $\varepsilon_0 = 2$, $\varepsilon_{s\geq 1} = 1$. For computational stability, the index s is chosen so that $|A_{2s}|$ is the largest. Similar expressions exist for the other families [23]. The Bessel and Hankel functions are computed for a complex argument.

The scattered wave is sought in the form of the series

$$W^{(s)} = \sum_m \left[a_m\, ce_m(\eta, q)\, Mc_m^{(3)}(\xi, q) + b_m\, se_m(\eta, q)\, Ms_m^{(3)}(\xi, q)\right]. \tag{13}$$

For complex q, the angular functions are orthogonal without complex conjugation: $\int_0^{2\pi} ce_m\, ce_n\, d\eta = 0$ $(m \neq n)$, since operator (9) is complex symmetric. Substituting (13) into boundary condition (7) and projecting onto ce_m (se_m), the coefficients are found separately:

$$a_m = -\frac{1}{N_m\, Mc_m^{(3)\prime}(\xi_0, q)} \int_0^{2\pi} \frac{\partial W^{(i)}}{\partial \xi}\Big|_{\xi_0} ce_m(\eta, q)\, d\eta, \qquad N_m = \int_0^{2\pi} ce_m^2\, d\eta. \tag{14}$$

The coefficients b_m are found in the same way. In (14), it is not necessary to expand the incident wave in Mathieu functions: the projection integral along the contour is evaluated directly by the trapezoidal rule, which gives exponential accuracy for periodic functions. The tangential stress along the contour is found as follows:

$$\tau_{\eta z}|_{\xi_0} = \frac{\mu^*}{c\, J} \frac{\partial}{\partial \eta}\left(W^{(i)} + W^{(s)}\right)|_{\xi_0}. \tag{15}$$

Normalization of the incident wave. In an elastic medium, the DSCF is defined as $K = \left|\tau_{\eta z}\right| / (\mu_0 k_0 W_0)$. In a viscoelastic medium, however, the amplitude of wave (8) varies along the propagation direction according to the law $e^{-Imk_* s}$. If W_0 is specified at the coordinate origin (at the center of the cavity), the amplitude at the point where the wave meets the cavity is $\exp(Imk_* d)$ times larger. For example, for $k_0 a = 6$, $\theta_0 = 0$ this factor equals 1.43. As a result, the DSCF is artificially increased. Therefore, in this paper the stress is normalized by the intensity of the wave at the point where it first touches the cavity:

$$K(\eta) = \frac{\left|\tau_{\eta z}\right|}{|\mu^* k_*|\; W_0\, e^{Imk_* d}}, \qquad d = \sqrt{a^2 \cos^2\theta_0 + b^2 \sin^2\theta_0}, \tag{16}$$

where d is the largest distance from the center to the contour in the direction perpendicular to the wave front. In the elastic case, (16) reduces to the usual definition.

Numerical implementation. For each family, an N×N matrix with N = 60 is used. In the series, $M = 12 + 2.5\,|k_*|\,a$ terms are retained. The contour is discretized with 1024 nodes, and the derivative $\partial/\partial\eta$ is computed by the fast Fourier transform. The calculations were performed in Python (NumPy, SciPy). The computation time for a single frequency is less than 1 s.

4. Verification of the method

The correctness of the algorithm was verified in three independent ways.

1) **Residual of the Mathieu equation.** When the radial functions (12) for complex $q = (1.3 + 0.08i)^2$ were substituted into Equation (9), the relative residual did not exceed 10^{-7}; this value is limited by the finite-difference derivative error.

2) **Limiting cases.** As $k_0 a \to 0$, the solution must tend to the static result for an elliptic hole under antiplane shear [1]: $K_{\max} = 1 + a/b$ for $\theta_0 = 90°$ and $K_{\max} = 1 + b/a$ for $\theta_0 = 0$. As $b/a \to 1$, the solution reduces to the exact solution for a circular cavity in Bessel functions [1]. For example, for b/a = 0.9995 and $k_0 a = 0.5$; 1.0; 2.0, the difference did not exceed 0.03 %.

3) **Method of fundamental solutions (MFS)** [26]. Here the scattered field is represented by 400 sources $H_0^{(1)}(k_* r)$ located on a confocal ellipse inside the cavity, and condition (7) is satisfied by collocation.

Table 1. Static limit ($k_0 a = 0.01$) and comparison with the MFS

Case	Mathieu solution	Reference value	Difference
b/a = 0.2; $\theta_0 = 0$ (static)	1.2000	1.2000 (1 + b/a)	$< 10^{-4}$
b/a = 0.2; $\theta_0 = 90°$ (static)	6.0010	6.0000 (1 + a/b)	$2 \cdot 10^{-4}$
b/a = 0.5; $\theta_0 = 90°$ (static)	3.0006	3.0000	$2 \cdot 10^{-4}$
b/a = 0.8; $\theta_0 = 90°$ (static)	2.2505	2.2500	$2 \cdot 10^{-4}$
$k_0 a = 1.0$; b/a = 0.4; $\theta_0 = 0$; elastic	1.387506	1.387506 (MFS)	$6 \cdot 10^{-13}$
$k_0 a = 1.5$; b/a = 0.2; $\theta_0 = 60°$; v.-el.	4.625906	4.625906 (MFS)	$3 \cdot 10^{-12}$
$k_0 a = 3.0$; b/a = 0.4; $\theta_0 = 0$; v.-el.	1.608579	1.608579 (MFS)	$2 \cdot 10^{-13}$
$k_0 a = 5.0$; b/a = 0.7; $\theta_0 = 90°$; v.-el.	1.647652	1.647652 (MFS)	$2 \cdot 10^{-13}$

The small difference in the static case is due to $k_0 a = 0.01$ being nonzero. The agreement with the MFS is close to machine precision. The fact that these two entirely different methods give the same result shows that algorithm (12)–(14) is correct. In Table 1, K is normalized at the coordinate origin, since the comparison was carried out in the same way for both methods.

5. Numerical results and discussion

The main kernel parameters adopted in the calculations are A = 0.048, $\alpha = 0.1$ and $\beta = 0.05$ ($\int_0^\infty R\,dt = 0.616$). Table 2 gives the corresponding complex modulus and wavenumber. These values of the kernel parameters were used in problems of wave propagation in viscoelastic cylindrical cavities [27].

Table 2. Complex modulus and wavenumber for the Rzhanitsyn–Koltunov kernel (A = 0.048; $\alpha = 0.1$; $\beta = 0.05$)

$k_0 a$	Γ_c	Γ_s	$\mathrm{Re}(k_*/k_0)$	$\mathrm{Im}(k_*/k_0)$	$\tan\delta$
0.1	0.5650	0.0628	1.5046	0.1081	0.144
0.5	0.4839	0.0717	1.3820	0.0955	0.139
1.0	0.4513	0.0692	1.3421	0.0843	0.126
2.0	0.4210	0.0656	1.3079	0.0738	0.113
4.0	0.3927	0.0617	1.2783	0.0648	0.102
6.0	0.3771	0.0594	1.2627	0.0601	0.095

Table 2 shows that viscosity has two effects. First, owing to Γ_c the modulus decreases and the wave slows down: the value of $Re k_*$ is 26–50 % greater than k_0. Second, owing to Γ_s the wave decays.

Effect of normalization. If K is normalized at the coordinate origin, then for b/a = 0.5, $\theta_0 = 0$ at $k_0 a = 6$ the DSCF in the viscoelastic medium is 26.8 % greater than in the elastic case (1.949 versus 1.537). This result leads to the incorrect conclusion that "viscosity increases the stress". With normalization (16), in the same case the DSCF decreases by 11.5 % (1.360). Hence, in damping media, conclusions about the DSCF depend significantly on the normalization method. All subsequent results are given according to (16).

Effect of the ellipse shape and incidence angle. Figure 2 shows the frequency dependence of the maximum DSCF along the contour ($K_{\max}$).

When the wave is incident along the minor axis ($\theta_0 = 90°$), the DSCF is large and increases sharply as the ellipse becomes thinner: for b/a = 0.3, $K_{\max}$ reaches 4.93. In all cases, $K_{\max}$ attains its largest value in the long-wave range ($k_0 a < 1$), and in an elastic medium it is 6–14 % greater than its static value. This result agrees qualitatively with the conclusions of [4] and [20, 21]. For $\theta_0 = 0$, the DSCF lies in the range 1.3–1.9 and depends weakly on frequency.

Table 3. Maximum DSCF and the effect of viscosity (A = 0.048; $\alpha = 0.1$; $\beta = 0.05$)

b/a	θ_0	$K_{\max}$ **(elastic)** / $k_0 a$	$K_{\max}$ **(viscoelastic)** / $k_0 a$	**Change of peak**	**Largest decrease** / $k_0 a$
0.3	90°	4.929 / 0.70	4.704 / 0.44	–4.6 %	–29.3 % / 1.30
0.5	90°	3.285 / 0.58	3.149 / 0.34	–4.2 %	–25.3 % / 1.15
0.8	90°	2.387 / 0.44	2.297 / 0.24	–3.8 %	–22.6 % / 1.00
0.3	0	1.317 / 2.35	1.299 / 0.02	–1.3 %	–13.8 % / 1.00
0.5	0	1.532 / 0.46	1.500 / 0.02	–2.1 %	–16.8 % / 1.05
0.8	0	1.867 / 0.40	1.806 / 0.16	–3.3 %	–20.6 % / 1.00

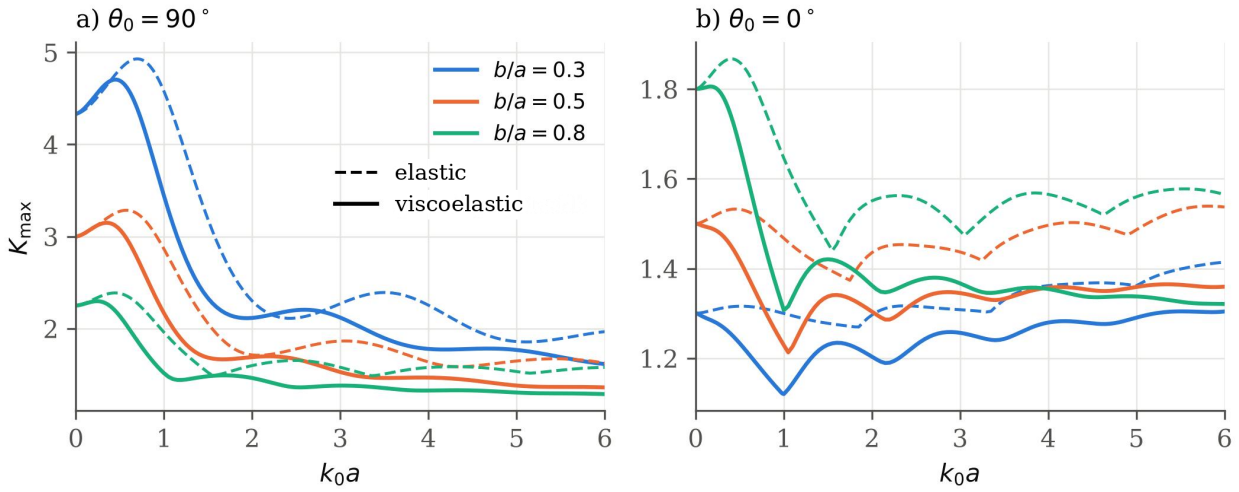


Figure 2. K_{max} as a function of k_0a: a) $\theta_0 = 90°$ (the wave is incident along the minor axis); b) $\theta_0 = 0$ (the wave is incident along the major axis). Dashed lines: elastic medium; solid lines: viscoelastic medium

An important conclusion can be drawn from Table 3: viscosity reduces the *peak value* of the DSCF by only 1–5 %, but shifts it *towards lower frequencies* (for $\theta_0 = 90°$ the peak frequency decreases by 37–45 %). Therefore, at a fixed frequency, especially near $k_0a \approx 1$, the DSCF decreases by 14–29 %.

Separating the effect of viscosity. To determine the contributions of the two mechanisms, an additional calculation was performed in which only the real part of μ^* was retained ($\Gamma_s = 0$), i.e. the medium softens but the wave does not decay (Figure 3).

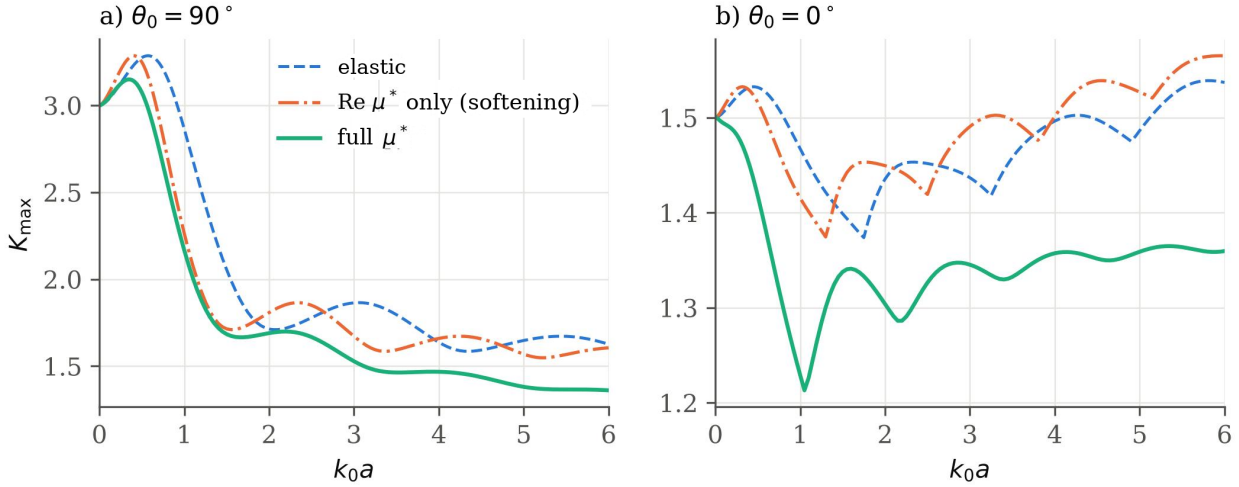


Figure 3. Separating the effect of viscosity (b/a = 0.5): dashed line, elastic medium; dash-dotted line, modulus reduction only ($Re\mu^*$); solid line, full complex modulus

Figure 3 shows that under the effect of Γ_c the curve K_{max} (k_0a) shifts to the left while almost retaining its shape. For $\theta_0 = 90°$, the peak moves from $k_0a = 0.58$ to 0.40, while the peak value does not change (3.285). The reason is that the DSCF depends on the actual wavelength, and since $Rek_* > k_0$, the wave is shorter at the same frequency. Damping (Γ_s) directly reduces the DSCF, and this effect increases with frequency: 4–5 % at $k_0a = 0.4$, 4–13 % at $k_0a = 1$, and 11–15 % at $k_0a = 5$–6. Thus, at low frequencies the effect of viscosity manifests itself mainly through the shift of the spectrum, and at high frequencies mainly through damping.

It should be noted that, for comparison, the elastic medium was taken with the instantaneous modulus μ_0. If the storage modulus $Re\mu^*$ at each frequency is taken as the elastic medium (the dash-dotted line in Figure 3), the spectrum shift disappears and the net effect of viscosity manifests itself only through damping (Γ_s). Therefore, the results on the spectrum shift are given relative to the instantaneous modulus.

Effect of the relaxation kernel parameters. Figure 4 and Table 4 present the results obtained when the kernel parameters are varied one at a time for b/a = 0.5, $\theta_0 = 90°$.

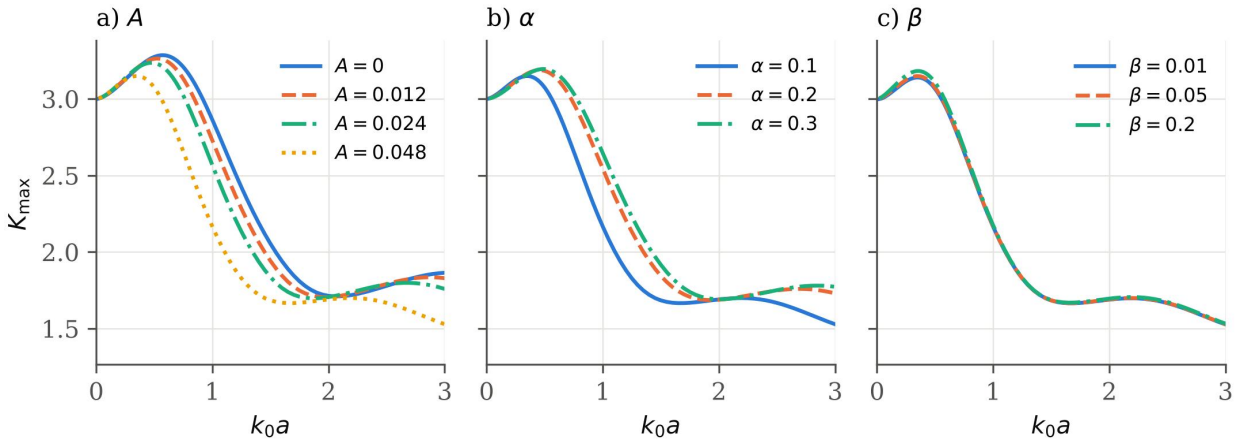


Figure 4. K_{max} as a function of the kernel parameters (b/a = 0.5; $\theta_0 = 90°$): a) A ($\alpha = 0.1$; $\beta = 0.05$); b) α (A = 0.048; $\beta = 0.05$); c) β (A = 0.048; $\alpha = 0.1$)

Table 4. Effect of the kernel parameters on the DSCF (b/a = 0.5; $\theta_0 = 90°$)

A	α	β	$\int R\,dt$	$\Gamma_c(1)$	$\Gamma_s(1)$	K_{max}/k_0a	$K(k_0a=1)$	$K(k_0a=3)$
0	–	–	0	0	0	3.285 / 0.58	2.863	1.864
0.012	0.1	0.05	0.154	0.113	0.017	3.263 / 0.52	2.728	1.829
0.024	0.1	0.05	0.308	0.226	0.035	3.235 / 0.48	2.567	1.759
0.048	0.1	0.05	0.616	0.451	0.069	3.149 / 0.34	2.166	1.528
0.048	0.2	0.05	0.401	0.210	0.066	3.187 / 0.46	2.543	1.730
0.048	0.3	0.05	0.353	0.129	0.063	3.194 / 0.48	2.646	1.773
0.048	0.1	0.01	0.724	0.451	0.071	3.139 / 0.34	2.164	1.527
0.048	0.1	0.2	0.536	0.452	0.062	3.182 / 0.36	2.174	1.532

The following regularities follow from Table 4:

– **Parameter A** increases Γ_c and Γ_s proportionally. As A increases, the DSCF spectrum shifts monotonically to the left and decreases: for A = 0.048, the DSCF at $k_0a = 1$ decreases by 24.3 %.

– As **parameter** α increases (with A and β fixed), $\Gamma_s(1)$ hardly changes (0.069 → 0.063), but $\Gamma_c(1)$ decreases by a factor of 3.5 (0.451 → 0.129). Therefore, α acts mainly through the modulus reduction (spectrum shift). When α changes from 0.1 to 0.2, the decrease at $k_0a = 1$ falls from 24 % to 11 %.

– The effect of **parameter** β is very small. When β changes by a factor of 20, K_{max} changes by 1.4 %, and the DSCF at a fixed frequency by less than 0.5 %. The reason is that at the computational frequencies $\omega \gg \beta$, so in (4) $\left(\beta^2 + \omega^2\right)^{\alpha/2} \approx \omega^\alpha$ and $\varphi \approx \pi/2$. β matters only at very low frequencies ($\omega \lesssim \beta$).

Thus, in practical calculations it is important to determine the kernel parameters A and α accurately from experimental data, whereas the parameter β may be specified approximately.

Stress distribution along the contour is shown in Figure 5 (ϑ is the polar angle of the contour point).

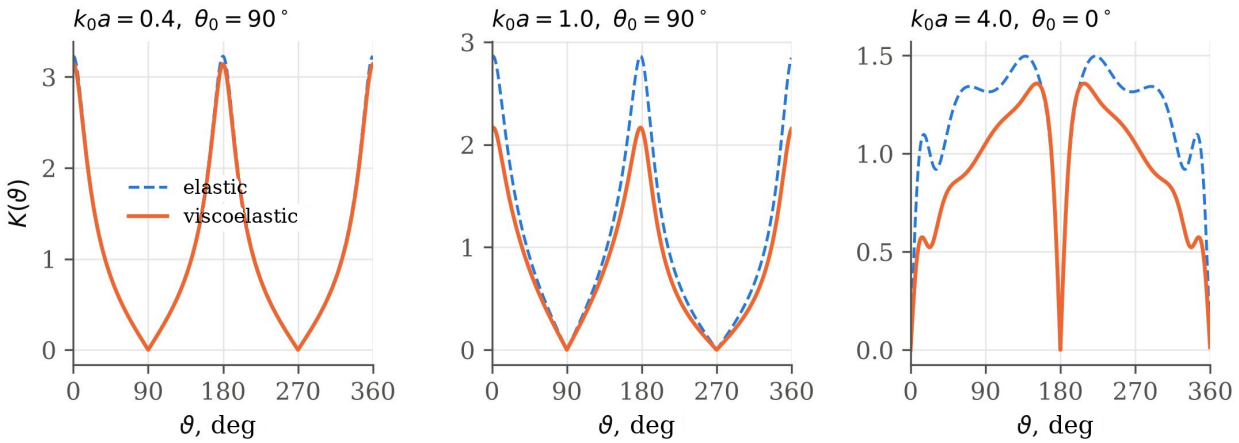


Figure 5. Distribution of the DSCF along the contour (b/a = 0.5). Dashed line: elastic medium; solid line: viscoelastic medium

For $\theta_0 = 90°$, the largest stress occurs at the ends of the major axis ($\vartheta = 0°, 180°$), while at the ends of the minor axis ($\vartheta = 90°, 270°$) the stress is zero. At $k_0 a = 0.4$, the viscoelastic and elastic distributions practically coincide. At $k_0 a = 1$, under the effect of viscosity the peaks decrease from 2.86 to 2.17, while the shape of the distribution is preserved. For $\theta_0 = 0$, $k_0 a = 4$, the elastic distribution has several local maxima due to interference. In the viscoelastic medium these oscillations are smoothed by damping, and the maximum shifts towards the incident wave: $\vartheta \approx 138°, 222°$ in the elastic case and $\vartheta \approx 151°, 209°$ in the viscoelastic case (the wave first touches the point $\vartheta = 180°$).

6. Filled elliptic cylinder

In real structures, the cavity is often filled: a concrete lining, injected soil, a plug, etc. Suppose that the ellipse is filled with a homogeneous viscoelastic material with shear modulus μ_2^* and density ρ_2, which is rigidly bonded to the medium. The parameters of the medium are denoted by the index 1. The field in the filler satisfies the Helmholtz equation of form (5) with the wavenumber

$$k_2 = k_0 \sqrt{\frac{\rho_2 \mu_{1,0}}{\rho_1 \mu_{2,0}}} \frac{1}{\sqrt{1 - \Gamma_c^{(2)} - i\,\Gamma_s^{(2)}}}, \tag{17}$$

where $\Gamma_{c,s}^{(2)}$ are the Fourier transforms of the filler kernel. The field in the filler must be bounded inside the ellipse:

$$W^{(2)} = \sum_m \left[c_m\, ce_m(\eta, q_2)\; Mc_m^{(1)}(\xi, q_2) + d_m\, se_m(\eta, q_2)\; Ms_m^{(1)}(\xi, q_2) \right], \qquad q_2 = \left(\frac{k_2 c}{2} \right)^2, \tag{18}$$

where $Mc_m^{(1)}$, $Ms_m^{(1)}$ are the radial Mathieu functions of the first kind (J is taken instead of $H^{(1)}$ in (12)). The displacement and stress are continuous at the interface:

$$W^{(i)} + W^{(s)} = W^{(2)}, \qquad \mu_1^* \frac{\partial}{\partial \xi} \left(W^{(i)} + W^{(s)} \right) = \mu_2^* \frac{\partial W^{(2)}}{\partial \xi}, \qquad \xi = \xi_0. \tag{19}$$

Unlike the cavity case, the inner and outer Mathieu functions have different parameters ($q_1 \neq q_2$). Therefore, they are not mutually orthogonal, and the coefficients cannot be found separately. Conditions (19) are written at 1024 points along the contour. The resulting overdetermined linear system is solved by the least-squares method after normalizing its columns. In all calculations, the residual did not exceed $5 \cdot 10^{-13}$. Two stress components in the medium are evaluated: the tangential stress $\tau_{\eta z}$ and the contact stress $\tau_{\xi z}$ (on the area normal to the ellipse). They are normalized as in (16) and denoted by K_η and K_ξ.

Verification. As b/a $\to$ 1, the solution agreed with the exact solution for a circular filler in Bessel functions (difference less than 0.02 %). As $\mu_2, \rho_2 \to 0$, the cavity result was recovered. In the static limit, the contact stress agrees with the classical solution of the antiplane problem $K_\xi = \varkappa(a+b)/(\varkappa a + b)$, $\varkappa = \mu_2/\mu_1$: for $\varkappa = 0.2$; 2; 10, the values 0.429; 1.200; 1.427 were obtained (exact values 0.429; 1.200; 1.429). In comparison with the method of fundamental solutions with sources placed on both sides of the contour, the difference did not exceed $3 \cdot 10^{-13}$.

Results. The calculations were performed for b/a = 0.5, $\theta_0 = 90°$, $\rho_2 = \rho_1$. The medium kernel is $A_1 = 0.048$; $\alpha = 0.1$; $\beta = 0.05$. The filler is also a viscoelastic material with the Rzhanitsyn–Koltunov kernel; in its kernel, α and β are the same as for the medium, and A_2 takes the values 0.012; 0.024; 0.048; 0.072 (in all cases $\int_0^\infty R\,dt < 1$). For comparison, the case in which both materials are elastic was also calculated.

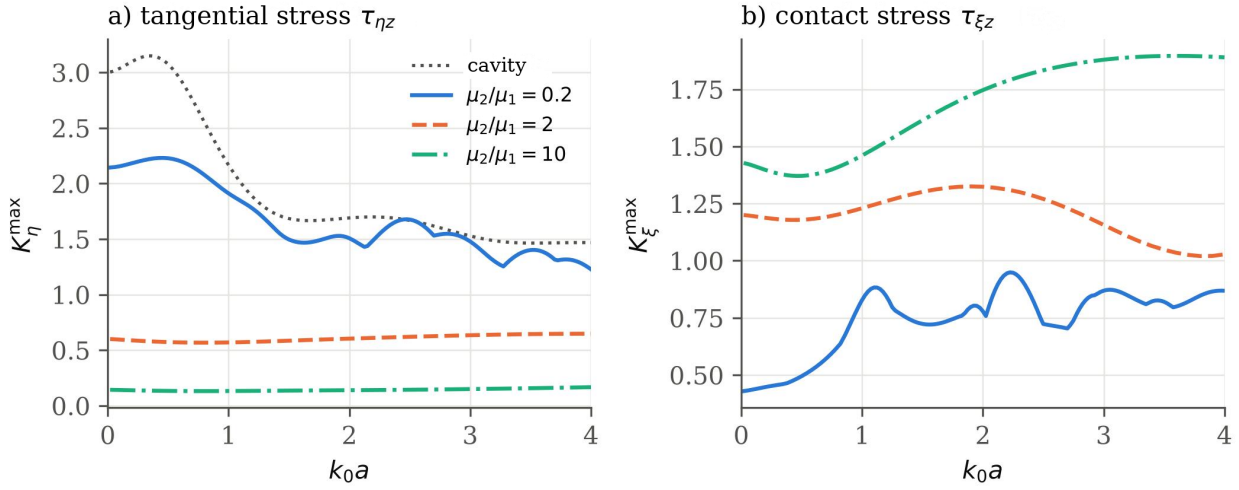


Figure 6. Effect of the filler stiffness (b/a = 0.5; $\theta_0 = 90°$; both materials viscoelastic): a) tangential stress K_η; b) contact stress K_ξ

Figure 6 shows that the filler fundamentally changes the stress state. A soft filler ($\varkappa = 0.2$) reduces the maximum tangential stress by 29 % relative to the cavity (from 3.149 to 2.230). In a stiff filler ($\varkappa \geq 2$), the tangential stress is small ($K_\eta < 0.7$), and the contact stress $\tau_{\xi z}$ becomes the main dangerous component. Its largest value ($K_\xi = 1.3$–1.9) occurs at the end of the minor axis on which the wave is incident ($\vartheta = 270°$). This stress may lead to detachment of the lining from the soil. In a stiff filler, K_ξ increases with frequency: at $\varkappa = 10$ it increases by 33 % relative to its static value (1.43) and reaches 1.90.

Table 5. DSCF in the filled cylinder (b/a = 0.5; $\theta_0 = 90°$; $0 < k_0a \le 4$; $A_1 = 0.048$)

$\varkappa = \mu_2/\mu_1$	**Filler**	**Component**	$k_0a = 0.02$	**Largest /** k_0a	$k_0a = 1$	$k_0a = 2$
0 (cavity)	medium elastic	K_η	3.000	3.285 / 0.58	2.863	1.713
0 (cavity)	medium v.-el.	K_η	3.000	3.149 / 0.34	2.166	1.690
0.2	both elastic	K_η	2.144	2.759 / 3.75	2.268	1.826
0.2	$A_2 = 0.012$	K_η	1.605	1.862 / 0.58	1.726	1.290
0.2	$A_2 = 0.024$	K_η	1.752	1.969 / 0.54	1.782	1.381
0.2	$A_2 = 0.048$	K_η	2.144	2.230 / 0.46	1.911	1.507
0.2	$A_2 = 0.072$	K_η	2.760	2.760 / 0.02	2.011	1.625
2	both elastic	K_ξ	1.200	1.351 / 2.60	1.190	1.317
2	$A_2 = 0.012$	K_ξ	1.345	1.547 / 2.25	1.346	1.536
2	$A_2 = 0.024$	K_ξ	1.315	1.484 / 2.15	1.317	1.481
2	$A_2 = 0.048$	K_ξ	1.200	1.325 / 1.90	1.229	1.324
2	$A_2 = 0.072$	K_ξ	0.734	1.122 / 1.85	1.069	1.120
10	both elastic	K_ξ	1.428	1.920 / 4.00	1.381	1.622
10	$A_2 = 0.012$	K_ξ	1.465	1.978 / 4.00	1.487	1.786
10	$A_2 = 0.024$	K_ξ	1.458	1.959 / 4.00	1.481	1.777
10	$A_2 = 0.048$	K_ξ	1.427	1.896 / 3.60	1.460	1.746
10	$A_2 = 0.072$	K_ξ	1.244	1.771 / 3.10	1.409	1.672

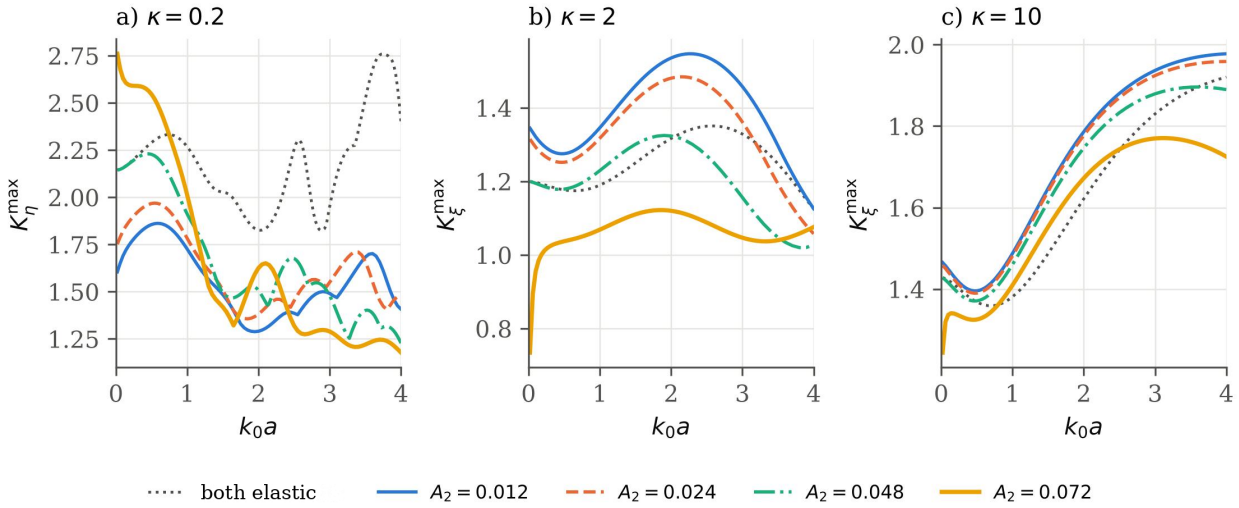


Figure 7. Effect of the filler viscosity (A_2), $A_1 = 0.048$ (b/a = 0.5; $\theta_0 = 90°$): a) soft filler, tangential stress; b), c) stiff filler, contact stress

Effect of the viscosity ratio. An important result follows from Figure 7 and Table 5: the stress state is determined not by the viscosity of the materials themselves but by the *ratio* of the filler and medium viscosities. This can be explained through the effective stiffness contrast:

$$\varkappa_{ef}(\omega) = \varkappa \frac{1 - \Gamma_c^{(2)}(\omega) - i\,\Gamma_s^{(2)}(\omega)}{1 - \Gamma_c^{(1)}(\omega) - i\,\Gamma_s^{(1)}(\omega)}. \tag{20}$$

For $A_2 = A_1$, $\varkappa_{ef} = \varkappa$ and the contrast does not depend on frequency. For $A_2 = 0.012$, the ratio $|\varkappa_{ef}|/\varkappa$ equals 1.95 at $k_0a = 0.1$ and 1.61 at $k_0a = 1$. For $A_2 = 0.024$ this ratio is 1.63 and 1.40, and for $A_2 = 0.072$ it is 0.41 and 0.61. As a result:

– **in a stiff filler** ($\varkappa = 2$), if the filler is less viscous than the medium, the contrast increases and the contact stress rises. The largest value of K_ξ is 16.8 % greater for $A_2 = 0.012$ (1.547) and 12.0 % greater for $A_2 = 0.024$ (1.484) than 1.325 for $A_2 = A_1$. If the filler is more viscous ($A_2 = 0.072$), it decreases by 15.3 % (1.122). At $\varkappa = 10$ the effect is weaker: +4.3 % and –6.6 %;

– **in a soft filler** ($\varkappa = 0.2$) the effect is the opposite: for $A_2 = 0.012$ the largest value of K_η decreases by 16.5 % (1.862), and for $A_2 = 0.072$ it increases by 23.8 % (2.760). In the latter case, the long-term modulus of the filler is very small, and at low frequencies it approaches a cavity.

Thus, unlike the cavity case, viscosity can either reduce or increase the stress at the filler boundary. Assigning the same kernel to both materials, or neglecting viscosity altogether, leads to underestimation of the contact stress by up to 17 %. Therefore, the kernel parameters of the filler and the medium must be determined separately.

In addition, when both materials are elastic, internal resonances are observed in the soft filler ($K_\eta = 2.3$–2.76 at $k_0a \approx 2.6$ and 3.75). The viscosity of the filler almost completely suppresses these resonance peaks (Figure 7, a).

7. Conclusions

1. An exact solution of the problem of SH-wave diffraction by an elliptic cavity in a viscoelastic medium was constructed in Mathieu functions of complex parameter. The computational algorithm is based on finding the Fourier coefficients from an eigenvalue problem, finding the Mathieu–Hankel functions from a series of products of Bessel functions, and determining the coefficients by projection along the contour. The algorithm was verified against the static limit, the circular-cavity solution and the method of fundamental solutions (agreement up to 10^{-12}).

2. It was found that normalizing the incident wave at the coordinate origin in a damping medium artificially overstates the DSCF by up to 27 % at high frequencies. Normalization (16) at the point where the wave first touches the cavity was proposed.

3. The effect of viscosity was separated into two mechanisms. The reduction of the elastic modulus (Γ_c) shifts the DSCF spectrum towards lower frequencies (for $\theta_0 = 90^\circ$ the peak frequency decreases by 37–45 %) and has almost no effect on the peak value. Damping (Γ_s) directly reduces the DSCF, and this effect increases with frequency up to 15 %.

4. When viscosity is taken into account, the largest value of the DSCF decreases by only 1–5 %, whereas at a fixed frequency ($k_0 a \approx 1$) it decreases by 14–29 %. Therefore, in the design of structures it is necessary to consider the entire frequency spectrum rather than only the peak value.

5. Of the Rzhanitsyn–Koltunov kernel parameters, A and α strongly affect the DSCF (α mainly through Γ_c). In the range of frequencies considered, the effect of β does not exceed 1.5 %.

6. The solution was generalized to a viscoelastic filled elliptic cylinder. In a stiff filler, the main dangerous component is the contact stress, which occurs at the end of the minor axis on which the wave is incident. The stress state is determined by the ratio of the filler and medium viscosities: through the effective contrast (20), the contact stress in a stiff filler varies from –15 % to +17 %, and the tangential stress in a soft filler from –17 % to +24 %. The viscosity of the filler suppresses its internal resonances.

Declarations

Author Contributions: R.A.S. is the sole author of the problem formulation, mathematical analysis, computational work, interpretation of results, and preparation and revision of the manuscript, as described in the submitted article. The author has approved the final version. (CRediT role assignment subject to author confirmation.)

Funding: This research received no external funding.

Ethics Approval: Not applicable. This study is an analytical and numerical investigation and does not involve human participants or live animals.

Informed Consent and Consent for Publication: Not applicable. No human participants or identifiable human information are reported in this study.

Data Availability Statement: The computational code and the numerical results obtained are available from the author upon reasonable request.

Acknowledgments: No additional acknowledgments were included in the submitted manuscript. The author should confirm this statement before publication.

Conflicts of Interest: The author declares no conflicts of interest.

Artificial Intelligence Disclosure: Artificial intelligence tools were used only for manuscript template formatting and translation into English. The problem formulation, solution method, calculations, results, and analysis were carried out by the author. The author reviewed the final text and takes full responsibility for the content.

Nomenclature and Abbreviations

Symbol / acronym	Definition
SH	Shear-horizontal (antiplane) wave
DSCF	Dynamic stress concentration factor
MFS	Method of fundamental solutions
a, b	Semi-axes of the elliptic cylinder/cavity
θ_0	Incident-wave angle
μ_0, μ^*	Instantaneous and complex shear moduli
ρ	Mass density
$R(t)$	Relaxation kernel of the viscoelastic material
A, α, β	Parameters of the Rzhanitsyn–Koltunov relaxation kernel
Γ_c, Γ_s	Cosine and sine Fourier transforms of the relaxation kernel
ω, c_0	Angular frequency and reference shear-wave speed
k_0, k_*, k_2	Reference, complex medium and filler wavenumbers
ξ, η, q	Elliptic coordinates and Mathieu parameter
$K, K_{\max}$	Local and maximum dynamic stress concentration factors
K_η, K_ξ	Tangential and interface-normal stress concentration measures
$\varkappa$	Filler-to-medium stiffness (shear modulus) ratio

$\tau_{\eta z}, \tau_{\xi z}$	Tangential and interface-normal shear stresses
Re, Im	Real and imaginary parts of a complex quantity

References

[1] Pao YH, Mow CC. Diffraction of Elastic Waves and Dynamic Stress Concentrations. Crane, Russak; 1973.

[2] Guz' AN, Kubenko VD, Čerevko MA. Difrakciâ uprugih voln [Diffraction of elastic waves]. Naukova Dumka; 1978. (In Russian).

[3] Chen Z, Liu D, Yang Z. Dynamic stress concentration and scattering of SH-wave by interface elliptic cylindrical cavity. Earthq Eng Eng Vib. 2003;2(2):299–306. https://doi.org/10.1007/s11803-003-0013-9.

[4] Tao M, Zhao R, Du K, Cao W, Li Z. Dynamic stress concentration and failure characteristics around elliptical cavity subjected to impact loading. Int J Solids Struct. 2020;191–192:401–417. https://doi.org/10.1016/j.ijsolstr.2020.01.009.

[5] Qi H, Chu F, Guo J. Dynamic analysis of non-confocal elliptical lined tunnel under the action of SH wave. Math Methods Appl Sci. 2022;45(7):3624–3643. https://doi.org/10.1002/mma.8008.

[6] Yang Z, Zhu Y, Ren H, Yang Y, Zhao J, Chen Y. Dynamic stress analysis of an elliptical cavity during elastic wave propagation in a density-inhomogeneous medium with the modulus varying as a power function. Eur J Mech A Solids. 2022;96:104740. https://doi.org/10.1016/j.euromechsol.2022.104740.

[7] Wang Z, Zhou C, Zhang X, et al. Magnetoacoustic wave scattering and dynamic stress concentration around the elliptical opening in exponential-gradient piezomagnetic materials. Materials (Basel). 2022;15(13):4564. https://doi.org/10.3390/ma15134564.

[8] Yang Z, Guo D, Bian J, Yang Y. Scattering of SH waves by elliptical cavity and type-III crack in deep anisotropic geology. Soil Dyn Earthq Eng. 2024;182:108695. https://doi.org/10.1016/j.soildyn.2024.108695.

[9] Lu P, Wang Y, Liu R, et al. Mathematical modeling of dynamic stress concentration in piezoelectric materials with elliptical openings under SH waves. Actuators. 2025;14(3):121. https://doi.org/10.3390/act14030121.

[10] Hu H, Szekrényes A, Dai M, Gao CF. Scattering of harmonic P-wave and dynamic stress concentration by a nanosized elliptical hole with surface effect. Math Mech Solids. Published online 2026. https://doi.org/10.1177/10812865261422754.

[11] Pillai TAK, Varadan VV, Varadan VK. Sound scattering by rigid and elastic infinite elliptical cylinders in water. J Acoust Soc Am. 1982;72(3):1032–1037.

[12] Scharstein RW, Davis AMJ. Acoustic scattering by a rigid elliptic cylinder in a slightly viscous medium. J Acoust Soc Am. 2007;121(6):3300–3310.

[13] Hasheminejad SM, Sanaei R. Ultrasonic scattering by a fluid cylinder of elliptic cross section, including viscous effects. IEEE Trans Ultrason Ferroelectr Freq Control. 2008;55(2):391–404.

[14] Koltunov MA. Polzučest' i relaksaciâ [Creep and relaxation]. Vysšaâ Škola; 1976. (In Russian).

[15] Rabotnov ÛN. Èlementy nasledstvennoj mehaniki tvërdyh tel [Elements of the hereditary mechanics of solids]. Nauka; 1977. (In Russian).

[16] Filatov AN. Asimptotičeskie metody v teorii differencial'nyh i integro-differencial'nyh uravnenij [Asymptotic methods in the theory of differential and integro-differential equations]. Fan; 1974. (In Russian).

[17] Safarov II, Ahmedov MŠ, Umarov AO. Dinamičeskie naprâženiâ i smeŝeniâ vblizi cilindričeskoj podkreplënnoj polosti ot ploskoj garmoničeskoj volny [Dynamic stresses and displacements near a reinforced cylindrical cavity due to a plane harmonic wave]. Prospero. 2014;(3):57–61. (In Russian).

[18] Ruziyev T, Safarov I, Teshayev M, et al. Assessment of the dissipative properties of viscoelastic hollow cylindrical bodies with filler during the propagation of natural waves. J Compos Sci. 2026;10(8):437. https://doi.org/10.3390/jcs10080437.

[19] Axmedov OS. Diffraction of a harmonic wave propagating through an elliptical cylinder in a viscoelastic medium. Theor Appl Sci. 2025;142(2):10–13.

[20] Axmedov OS. Qovushqoq-elastik to'ldiruvchili elliptik silindrik qobiqqa garmonik to'lqin tarqalishini Matye funksiyalardagi yechimi [Solution in Mathieu functions for harmonic wave propagation in a viscoelastic filled elliptic cylindrical shell]. BuxDU Ilmiy Axboroti. 2025;(2):7–12. (In Uzbek).

[21] Axmedov OS. Qovushqoq-elastik elliptik silindrga bo'ylama va ko'ndalang garmonik to'lqin difraksiyasi [Diffraction of longitudinal and transverse harmonic waves by a viscoelastic elliptic cylinder]. Ilm Sarchashmalari. 2025;(12):7–13. (In Uzbek).

[22] McLachlan NW. Theory and Application of Mathieu Functions. Clarendon Press; 1947.

[23] National Institute of Standards and Technology. NIST Digital Library of Mathematical Functions. Chapter 28: Mathieu functions and Hill's equation. Accessed October 6, 2026. https://dlmf.nist.gov/28.

[24] Alhargan FA. Algorithm 804: subroutines for the computation of Mathieu functions of integer orders. ACM Trans Math Softw. 2000;26(3):390–407. https://doi.org/10.1145/358407.358422.

[25] Brimacombe C, Corless RM, Zamir M. Computation and applications of Mathieu functions: a historical perspective. SIAM Rev. 2021;63(4):653–720. https://doi.org/10.1137/20M135786X.

[26] Fairweather G, Karageorghis A. The method of fundamental solutions for elliptic boundary value problems. Adv Comput Math. 1998;9:69–95.

[27] Teshaev MKh, Safarov II, Kuldashov NU, Ishmamatov MR, Ruziev TR. On the distribution of free waves on the surface of a viscoelastic cylindrical cavity. J Vib Eng Technol. 2020;8(4):579–585. https://doi.org/10.1007/s42417-019-00160-x.

Disclaimer of Liability/Publisher's Note

The statements, opinions, and data contained in all publications are solely those of the individual author(s) and contributor(s) and do not necessarily reflect the views of the Publisher, the Journal, or the editors. The Publisher, the Journal, and the editors disclaim responsibility for any injury to persons or damage to property resulting from any ideas, methods, instructions, or products referred to in the content.